Journal of Alloys and Compounds 509 (2011) 6262–6266

Contents lists available at ScienceDirect

Journal of Alloys and Compounds

journal homepage: www.elsevier.com/locate/jallcom

Fabrication and luminescence properties of In_2O_3-capped ZnS nanowires

Sunghoon Park[a], Changhyun Jin[a], Hyoun Woo Kim[b], Chongmu Lee[a,*]

[a] Department of Materials Science and Engineering, Inha University, Yonghyeondong, Incheon, 402-751, Republic of Korea
[b] Division of Materials Science and Engineering, Hanyang University, 17 Haengdang, Seongdong-gu, Seoul 133-791, Republic of Korea

ARTICLE INFO

Article history:
Received 24 December 2010
Received in revised form 2 March 2011
Accepted 6 March 2011
Available online 16 March 2011

Keywords:
ZnS nanowires
Annealing
Energy-dispersive X-ray spectroscopy
Photoluminescence spectroscopy

ABSTRACT

ZnS-core/In_2O_3-shell nanowires have been prepared by using a two-step process: thermal evaporation of ZnS powders on Si(1 0 0) substrates coated with Au thin films and sputter-deposition of In_2O_3. The ZnS nanowires were a few tens of nanometers in diameter and a few hundreds of micrometers in length. ZnS nanowires have an emission band centered at approximately 570 nm in the yellow region. The yellow emission has been enhanced in intensity by capping the ZnS nanowires with In_2O_3 presumably due to the increase in the concentrations of indium and oxygen interstitials in the very surface region of the ZnS cores and further enhanced by annealing in a reduction atmosphere maybe because of the increase in the concentration of Au_{Zn}^{-} in the ZnS cores. In contrast, the yellow emission intensity has been decreased by annealing in an oxidation atmosphere due to the conversion of ZnS into ZnO as a result of the reaction of ZnS in the cores with oxygen.

1. Introduction

Zinc Sulfide (ZnS) is an important II–VI semiconductor with a wide direct energy band gap (3.7 eV) at room temperature having received significant attention over the past few decades. ZnS has potential applications in flat panel displays, infrared windows, ultraviolet light-emitting diodes and injection lasers, phosphors in cathode-ray tubes, electroluminescent thin film devices, and sensors owing to its intense luminescence, high refractive index, and high transmittance properties in the visible range [1,2]. ZnS is also promising for room temperature exciton devices since it has large exciton binding energy (38 meV) compared to the room temperature thermal energy (25 meV) [3]. Regarding ZnS one-dimensional (1D) nanostructures, a variety of techniques for the synthesis of ZnS nanowires have been reported. These techniques include thermal evaporation of ZnS powders [4], solvothermal process [5], chemical vapor deposition [6], electrochemical deposition [7], and template-assisted routes [8], etc. On the other hand, In_2O_3 is an important n-type wide band gap (3.55–3.75 eV, depending on the synthesis method) transparent conducting oxide material. Due to its high electrical conductivity, high transparency to the visible light, and intense interaction with some poisonous gases, In_2O_3 has been widely used in transparent conductive electrodes, optoelectronic devices such as solar cells, flat panel displays and gas sensors. 1D In_2O_3 nanostructures are also known to be sensitive to NO_2 and NH_3 gases as well as to biomolecules [9].

In recent years, 1D nanostructures such as nanowires, nanorods, nanobelts, nanoribbons, nanoneedles, nanotubes have attracted significant attention owing to their unique optical and electronic properties. A common technique to control and enhance the properties of the 1D nanostructures is to create core–shell coaxial heterostructures [10–13]. For example, the photoluminescence (PL) emission intensity of the light emitted from core–shell nanostructures can be increased significantly or the wavelength of the emission can be controlled by selecting a proper coating material and a proper coating layer thickness [14,15]. Capping ZnS 1D nanostructures with a metal oxide such as In_2O_3 is expected to result in prevention of the nanostructure from contamination as well as enhancement of the luminescence property of the nanostructures. The PL properties of ZnS and In_2O_3 1D nanostructures have been reported by many researchers in recent years. However, there have been no reports on the synthesis and PL properties of ZnS-core/In_2O_3-shell 1D nanostructures yet. In this paper, we report on the effects of capping and annealing, in particular, the annealing atmosphere on the PL properties of ZnS nanowires.

2. Experimental

We prepared ZnS-core/In_2O_3-shell nanowires on Si(1 0 0) substrates. Firstly, an Au thin film 3 nm thick was deposited onto the Si substrate by using an RF magnetron sputterer to prepare the Au-coated Si (1 0 0) substrate. The experimental apparatus used for synthesizing 1D ZnS nanostructures is a two-heating zone horizontal tube-furnace the schematic diagram of which is shown elsewhere [14]. ZnS powders in an alumina boat and the Si-substrate were placed separately in the two-heating zone-tube furnace, where the ZnS powders were in the first heating zone (Zone A) and the Si substrate in the second heating zone (Zone B). The substrate temperatures of zone A and zone B were set to 1000 and 850 °C, respectively, with the ambient nitrogen gas pressure and flow rate kept at 0.5 torr and

* Corresponding author. Tel.: +82 32 860 7536; fax: +82 32 862 5546.
E-mail address: cmlee@inha.ac.kr (C. Lee).

0925-8388/$ – see front matter.
doi:10.1016/j.jallcom.2011.03.043

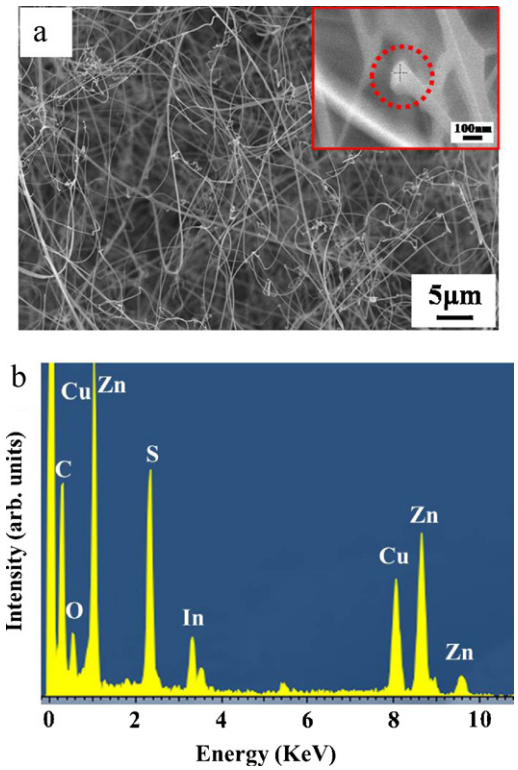

Fig. 1. (a) SEM image and (b) EDS spectrum of ZnS/In_2O_3 coaxial nanowires synthesized by a two-step process: the thermal evaporation of ZnS powders and the sputter-deposition of In_2O_3.

500 standard cm^3/min, respectively, throughout the synthesis process. The thermal evaporation process was conducted for 1 h and then the furnace was cooled down to room temperature.

Secondly, the ZnS nanowires were capped with In_2O_3 by sputtering. The sputter-deposition was done at room temperature using a 99.999% In_2O_3 target in a radio-frequency (rf) magnetron sputtering system. After the vacuum chamber was evacuated to 1×10^{-6} torr using a turbomolecular pump backed by a rotary pump. Ar gas was provided at a flow rate of 30 sccm. Deposition was carried out at room temperature for 15 min. The system pressure and rf sputtering power were 1.8×10^{-2} torr and 100 W, respectively. Subsequently the as-prepared core–shell nanowire samples were optionally annealed in an O_2 or N_2/3-mol% H_2 atmosphere at 600 °C for 1 h to see the influence of annealing on the PL properties of the wires.

Next, the prepared nanowire samples were characterized by using field emission scanning electron microscopy (FESEM, Hitachi S-4200 equipped with an energy dispersive X-ray spectrometer (EDXS)) and transmission electron microscopy (TEM, Phillips CM-200). The high resolution TEM (HRTEM) images and the selected area electron diffraction (SAED) patterns were also taken on the same systems. X-ray diffraction (XRD) analyses were performed at room temperature on the ZnS-core/In_2O_3-shell nanowire samples using an X-ray diffractometer (Philips X'pert MRD) with Cu-K_α radiation. The PL of the samples was measured at room temperature using a 325 nm He–Cd laser (Kimon, IK, Japan) as the excitation source.

3. Results and discussion

The SEM image of the as-synthesized ZnS-core/In_2O_3-shell nanowires is shown in Fig. 1(a). The core–shell nanowires were a few tens of nanometers in diameter and a few hundreds of micrometers in length. The enlarged SEM image of a typical core–shell nanowire (inset in Fig. 1(a)) clearly shows that a globular droplet or particle does exist at the tip of the nanowire. The EDX spectrum (Fig. 1(b)) taken from the particle in the enlarged SEM image (inset in Fig. 1(a)) shows that the particle comprises not only Zn, S, In and O but also Au elements. These two facts suggest that the ZnS nanowires have grown through a catalyst-assisted vapor–liquid–solid (VLS).

Fig. 3 shows the XRD patterns of the as-synthesized and annealed ZnS/In_2O_3 core–shell nanowires. The reflection peaks for

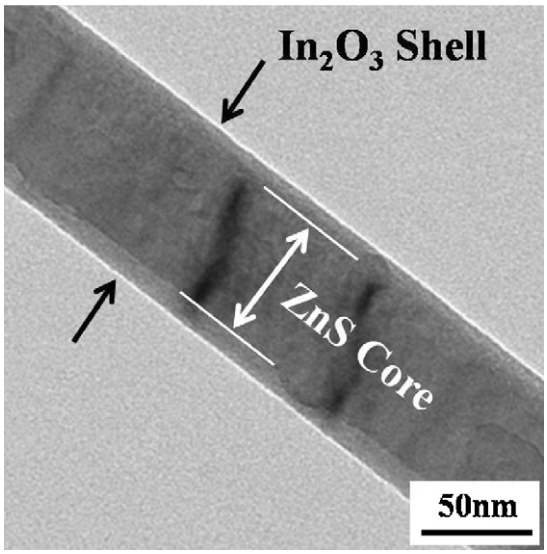

Fig. 2. Low-magnification TEM image of a typical ZnS/In_2O_3 coaxial nanowire.

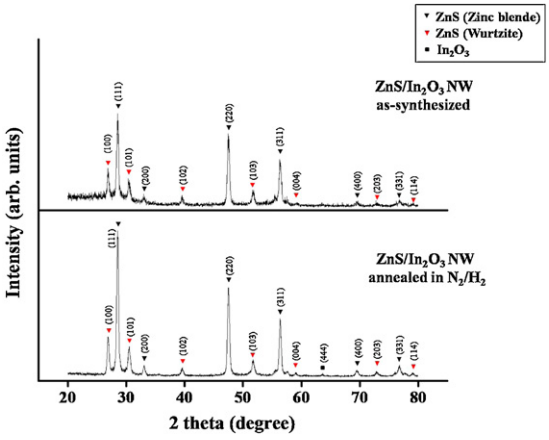

Fig. 3. XRD pattern of the ZnS/In_2O_3 coaxial nanowires after annealing.

ZnS nanowires are indexed as the lattice planes of zinc blende (JCPDS 77-2100) and wurtzite ZnS structures (JCPDS 89-2158), indicating that the cores of both the as-synthesized and annealed core–shell nanowires comprise both zinc blende and wurtzite-structured ZnS phases. Of these two phases, it appears that the former and the latter are a majority and a minority, respectively, because the reflection intensities of the former are much higher than those of the latter. On the other hand, no reflection peaks for In_2O_3 are observed in the XRD patterns for both the as-synthesized and annealed nanowires, suggesting that the In_2O_3 shells are amorphous even after annealing even if a very small In_2O_3 (444) reflection peak were observed for the annealed nanowires.

The low-magnification TEM image of a typical ZnS-core/In_2O_3-shell nanowire in Fig. 2 clearly shows a rod-like core (a dark area inside) and two shell layers (the less dark areas on both edge sides of the dark area) with a high thickness uniformity along the length of the nanowire. The thicknesses of the ZnS core and In_2O_3 shell layer are approximately 53 and 7–11 nm, respectively. The high-resolution TEM (HRTEM) image of the interfacial area of the core and shell of a typical ZnS-core/In_2O_3-shell nanowire and corresponding selected area electron diffraction (SAED) pattern are shown in Fig. 4(a) and (b), respectively. Two different sets of fringe pattern are observed in the ZnS core (Fig. 4(a)). The resolved spacings between the parallel fringes are about 0.31 and 0.19 nm, which

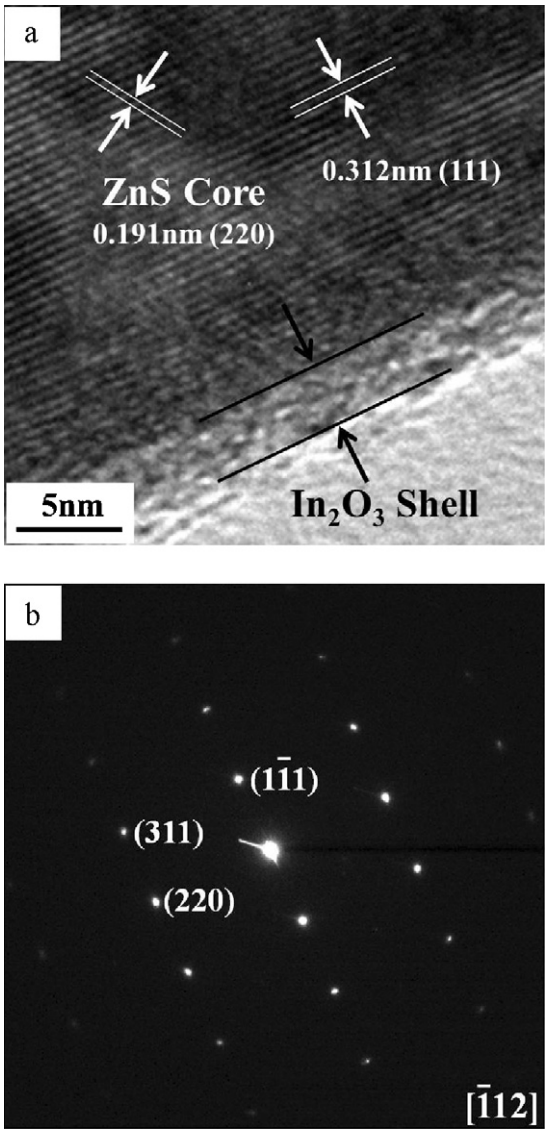

Fig. 4. (a) Local HRTEM image of a typical ZnS/In_2O_3 coaxial nanowire at the core–shell interface region. (b) SAED pattern of the [1$\bar{1}$0] zone axis of the nanomaterial at the same region as in (a).

are, respectively, in good agreement with the interplanar spacings of the (1 1 1) and (2 2 0) lattice planes of zinc blende ZnS with a lattice parameter of $a = 0.5414$ nm (JCPDS 77-2100). Both the HRTEM image (Fig. 4(a)) and corresponding SAED pattern taken along the [1$\bar{1}$0] zone axis (the inset of Fig. 4(a)) clearly indicate that the ZnS core is crystalline. On the other hand, a fringe pattern is not observable in the shell area of the annealed core–shell nanowire in the HRTEM image, which suggests that the In_2O_3 shells have not been crystallized completely by annealing maybe because annealing at 600 °C for 1 h was not sufficient for the In_2O_3 shells in the as-synthesized core–shell nanowires to be crystallized. This result is consistent with the XRD analysis result shown in Fig. 3.

Regarding the PL emissions of ZnS nanostructures, there have been many reports before [16–25]. These emissions are largely classified into five different groups in terms of the wavelength range or the origin of the emission: near-band edge (NBE) emission in a range of 320–370 nm, violet emission in a range of 390–400 nm, blue emission in a range of 430–470 nm, green emission in a range 510–550 nm, and an orange emission in a range of 600–620 nm. The NBE emission was reported for the wurtzite ZnS nanowires synthesized via vapor phase deposition [16] and solution routes [17]. The

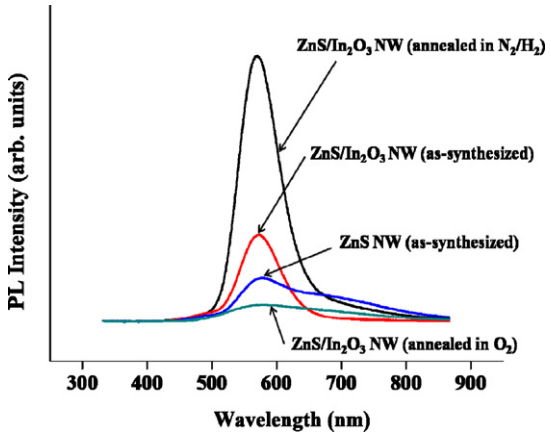

Fig. 5. Room temperature-PL spectra of the ZnS/In_2O_3 coaxial nanowires annealed at 600 °C for 1 h in different atmospheres along with the as-prepared ZnS/In_2O_3 coaxial nanowires.

NBE emission is known to originate from band-to-band transition since the band gap of ZnS (3.66 eV) corresponds to 330 nm [18]. The emission could be due to the excitonic transition [18] or the quantum size effect [19]. The violet emission is known to originate from deep levels like Zn^{2+} vacancies, interstitials, and dislocations [18,19]. The blue emission is reported to be associated with the trapped luminescence arising from the surface states, Zn^{2+} vacancies, and S^{2-} vacancies [17,20–25]. The green emission may be attributed to dopants or impurity atoms i.e., transitions from the conduction band of ZnS to the different levels of excited impurity atoms in the ZnS band gap [26,27]. It has also been suggested that a possible source for the green emission is Au^{+} ions substituting Zn^{2+} (Au_{Zn}^{-}) [28–30] formed as a result of Au diffusion from the Au thin film, used to catalyze the nanowire growth, into the ZnS nanowires [31–34]. The orange emission is due to deep levels [21]. On the other hand, it is well known that bulk In_2O_3 cannot emit light at room temperature [35]. However, Zhou et al. observed PL peaks at 480 and 520 nm from the In_2O_3 nanoparticles [36]. Lee et al. noticed a peak at 637 nm for In_2O_3 films [37]. Liang and coworkers observed a peak at 470 nm from In_2O_3 nanofibers [38] and recently Wu et al. reported two distinct peaks at 416 and 435 nm for In_2O_3 nanowires [39]. These emissions are commonly referred as the deep level emissions due to oxygen deficiencies.

The PL spectra of the ZnS-core/In_2O_3-shell nanowires annealed in different atmospheres are shown in Fig. 5 along with that of the as-synthesized (unannealed) ZnS and ZnS-core/In_2O_3-shell nanowires. The PL spectra of the nanowires are dominated by a deep level-related emission and the NBE emission is negligible. The deep level-related emission band is centered at approximately 570 nm in the yellow region on all the PL spectra of the four different kinds of nanowires. A yellow emission from ZnS nanowires has not been reported before, but the yellow emission from the ZnS nanowires synthesized in this work may also be attributed to impurity atoms like the green emission reported previously, more specifically speaking, Au^{+} ions substituting Zn^{2+} (Au_{Zn}^{-}) in the ZnS core.

Fig. 5 shows that the yellow emission intensity has been increased by coating them with In_2O_3. It is assumed that In and O atoms are sputtered into the very surface region of the ZnS nanowires during the sputter-deposition process of In_2O_3. These impurity atoms may reside at the interstitial sites of the ZnS nanowires. Further systematic investigation may be necessary, but it is surmised at present that the enhancement of the yellow emission by In_2O_3 coating is attributed to this increase in the concentrations of In and O interstitials in the very surface region of the ZnS core. The yellow emission intensity has been increased

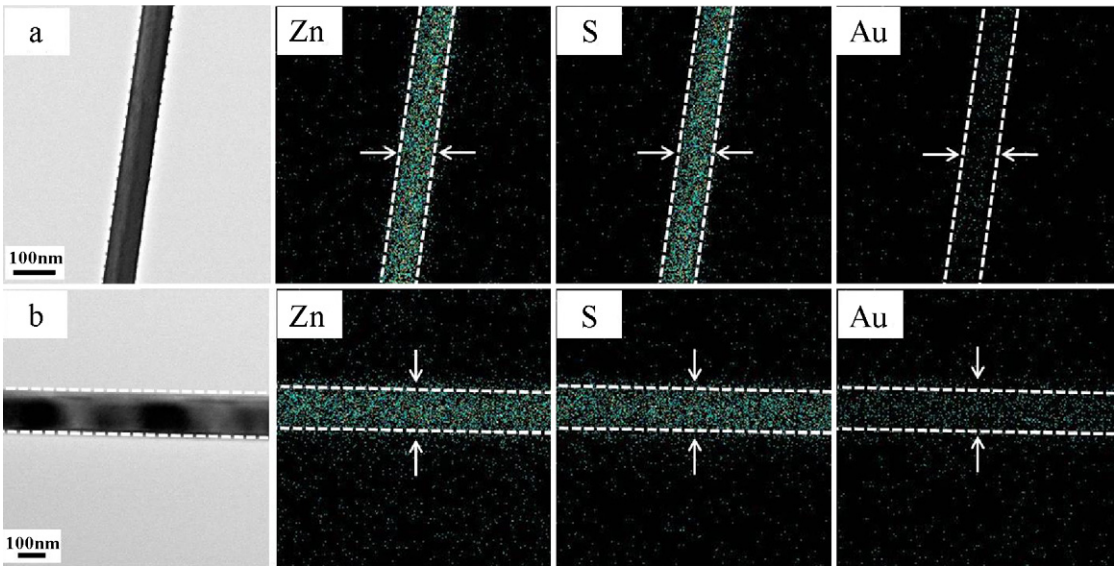

Fig. 6. EDS elemental maps of Au in the typical ZnS/In_2O_3 coaxial nanowires (a) before and (b) after annealing in an N_2/3 mol%-H_2 atmosphere.

further by annealing in a reduction atmosphere, but that it has been decreased by annealing in an oxidation atmosphere (Fig. 5). The EDXS elemental maps for the ZnS/In_2O_3 nanowire samples before and after annealing in an H_2/N_2 atmosphere are shown in Fig. 6(a) and (b), respectively. Close comparison of the Au elemental maps in Fig. 6(a) and (b) indicate that the annealed nanowire has a higher density of Au than the as-synthesized one. The white spots distributed along the length of the nanowires are Au atoms. Most of the Au atoms used as catalysts in the VLS growth exist at the tip of the as-synthesized nanowire as was shown in Fig. 1(a) although the tip area is not shown in Fig. 6(a). The Au atoms located at the tip of the nanowire may be redistributed during the thermal annealing process. Diffusion of Au atoms along the length of the nanowire occurs during annealing, which results in a decrease in the Au concentration at the tip but an increase in the Au concentration in the other areas of the nanowire. This does not necessarily mean that the Au_{Zn}^- concentration in the core is increased in the other areas of the nanowire by annealing but that the probability of substitution of Au^+ ions with Zn^{2+} is increased by annealing. As written above, Au_{Zn}^- is also a possible source for the yellow emission. At present, it is, however, not well understood why the Au_{Zn}^- concentration in the core is further increased by annealing in a reduction atmosphere compared to annealing in an oxidation atmosphere. Further study is necessary, but we surmise at present that the enhanced substitution of Zn atoms with Au atoms is associated with the higher concentration of S vacancies in the nanowires annealed in a reduction atmosphere. The unstable Zn atoms with dangling bonds due to neighboring S vacancies are more likely to be substituted by Au atoms.

On the other hand, the yellow emission intensity is decreased by annealing in the O_2 atmosphere, which may be caused by the conversion of ZnS into ZnO as a result of the following reaction occurring during the annealing process [40]:

$$2ZnS(s) + O_2(g) = 2ZnO(s) + S_2(l):$$

$$\Delta G_{f,873K} = -156.452\,KJ/mol \quad (1)$$

The defect-related deep-level emission from ZnO nanostructures are known to depend upon the preparation methods and growth conditions strongly, but the green emission at approximately 510 nm and the red emission at approximately 650 nm from ZnO nanostructures have been observed previously [36]. It is evident that only a portion of the ZnS in the cores have been converted into ZnO because no emissions characteristic of ZnO are observed for the core–shell nanowire sample annealed in the O_2 atmosphere. It is not certain at present what portion of the ZnS in the cores have been converted to ZnO during the annealing process, but it is clear that the amount of ZnS in the cores have been reduced by this reaction, which may be the cause of the degradation of the yellow emission in intensity by annealing in an O_2 atmosphere.

4. Conclusions

ZnS-core/In_2O_3-shell nanowires have been prepared by using a two-step process: thermal evaporation of ZnS powders on Si(1 0 0) substrates coated with Au thin films and sputter-deposition of In_2O_3. The ZnS nanowires grown by thermal evaporation are a few tens of nanometers in diameter and a few hundreds of micrometers in length. ZnS nanowires have an emission band centered at around 570 nm in the yellow region. The yellow emission is enhanced in intensity by coating the ZnS nanowires with In_2O_3 and further enhanced by annealing in a reduction atmosphere, but it is degraded by annealing in an oxidation atmosphere. The enhancement of the yellow emission by In_2O_3 coating may be attributed to this increase in the concentrations of In and O interstitials in the very surface region of the ZnS cores. On the other hand, a possible origin of the enhancement of the yellow emission in the ZnS/In_2O_3 nanowires by annealing in a reduction atmosphere is the redistribution of the Au^+ ions substituting Zn^{2+} (Au_{Zn}^-) in the ZnS core during the annealing process. In contrast, the degradation of the yellow emission in intensity by annealing in an O_2 atmosphere is caused by the conversion of ZnS into ZnO as a result of the reaction of ZnS in the cores with oxygen.

Acknowledgement

This work was supported by Korea Science and Engineering Foundation through '2010 Core Research Program'.

References

[1] T.V. Prevenslik, J. Lumin 1210 (2000) 87–89.
[2] T. Yamamoto, S. Kishimoto, S. Lida, Physica B 308 (2001) 916–919.
[3] S. Biswas, T. Ghoshal, S. Kar, S. Chakrabarti, S. Chaudhuri, Cryst. Growth Des. 8 (2008) 2171–2176.
[4] Y.Q. Li, K. Zou, Y.Y. Shan, J.A. Zapien, S.T. Lee, J. Phys. Chem. B 110 (2006) 6759–6762.

[5] L. Chai, J. Du, S. Xiong, H. Li, Y. Zhu, Y. Qian, J. Phys. Chem. C 111 (2007) 12658–12713.
[6] X.J. Xu, G.T. Fei, W.H. Yu, X.W. Wang, L. Chen, L.D. Zhang, Nanotechnology 17 (2006) 426–429.
[7] X.P. Shen, M. Han, J.M. Hong, Z.L. Xue, Z. Xu, Chem. Vap. Deposition 11 (2005) 250–253.
[8] Y. Liu, C. Zheng, W. Wang, Y. Zhau, G. Wang, J. Cryst. Growth 233 (2001) 8–12.
[9] A.M. Morales, C.M. Lieber, Science 279 (1998) 208–211.
[10] H.W. Kim, S.H. Shim, C. Lee, Mater. Sci. Eng. B 111 (2007) 148–153.
[11] Y. Yu, J. Xiang, C. Yang, W. Lu, C.M. Lieber, Nature 450 (2004) 61–65.
[12] L.J. Lauhon, M.S. Gudiksen, D. Wang, C.M. Lieber, Nature 420 (2002) 57–61.
[13] S. Park, H. Kim, J.W. Lee, H.W. Kim, C. Lee, J. Korean Phys. 53 (2008) 657–661.
[14] J. Jun, S. Park, J. Lee, C. Lee, J. Mater. Sci. Mater. Electron. 20 (2009) 1150–1153.
[15] J. Jun, C. Jin, H. Kim, J. Kang, C. Lee, Appl. Phys. A 96 (2009) 813–818.
[16] Y. Chang, M. Wang, X. Chen, S. Ni, W. Qiang, Solid State Commun. 142 (2007) 295–298.
[17] J. Zhang, Y. Yang, F. Jiang, J. Li, B. Xu, X. Wang, S. Wang, Nanotechnology 17 (2006) 2695–2699.
[18] W.G. Becker, A.J. Bard, J. Phys. Chem. 87 (1983) 4888–4893.
[19] S. Shionoya, in: P. Goldberg (Ed.), Luminescence of Inorganic solids, Academic, New York, 1966, pp. 206–277.
[20] A.A. Bol, A. Meijerink, J. Phys. Chem. B 105 (2001) 10203–10209.
[21] P. Hu, Y. Liu, L. Fu, L. Cao, D. Zhu, J. Phys. Chem. B 108 (2004) 936–938.
[22] D. Denzler, M. Olschewski, K. Sattler, J. Appl. Phys. 84 (1998) 2841–2845.
[23] Y.C. Zhu, Y. Bando, D.F. Xue, Appl. Phys. Lett. 82 (2003) 1769–1771.
[24] Y.W. Wang, L.D. Zhang, C.H. Liang, G.Z. Wang, X.S. Peng, Chem. Phys. Lett. 357 (2002) 314–318.
[25] P.H. Kasai, Y. Otomo, J. Phys. Chem. 87 (1962) 4888–4893.
[26] Y. Jiang, X.M. Meng, J. Liu, Z.Y. Xie, C.S. Lee, S.T. Lee, Adv. Mater. 15 (2003) 323–327.
[27] Y. Jiang, X.M. Meng, J. Liu, Z.R. Hong, C.S. Lee, S.T. Lee, Adv. Mater. 15 (2003) 1195–1198.
[28] S.T. Henderson, P.W. Ranby, M.B. Halstead, J. Electrochem. Soc. 106 (1959) 27–34.
[29] T. Hoshina, H. Kawai, Jpn. J. Appl. Phys. 19 (1980) 267–277.
[30] N.R.J. Poolton, J. Phys. C 20 (1987) 5867–5876.
[31] Q. Li, C. Wang, Appl. Phys. Lett. 83 (2003) 359–362.
[32] Y. Wang, L. Zhang, C. Liang, G. Wang, X. Peng, Chem. Phys. Lett. 357 (2002) 314–318.
[33] Q. Xiong, G. Chen, J.D. Acord, X. Liu, J.J. Zengei, H.R. Gutierrez, J.M. Redwing, L.C. Lew Yan Voon, B. Lassen, P.C. Eklund, Nano Lett. 4 (2004) 1663–1668.
[34] R.A. Rosenberg, G.K. Shenoy, F. Heigl, S.T. Lee, P.S.G. Kim, X.T. Zhou, T.K. Sham, Appl. Phys. Lett. 86 (2005) 263115.
[35] X.C. Wu, J.M. Hong, Z.T. Han, Y.R. Tao, Chem. Phys. Lett. 373 (2003) 28–32.
[36] C. Liang, G. Meng, Y. Lei, F. Phillipp, L. Zhang, Adv. Mater. 13 (2001) 1330–1333.
[37] P. Guha, S. Kar, S. Chaudhuri, Appl. Phys. Lett. 85 (2004) 3851–3853.
[38] H.J. Zhou, W.P. Cai, L.D. Zhang, Appl. Phys. Lett. 75 (1999) 495–497.
[39] M.S. Lee, W.C. Choi, E.K. Kim, C.K. Kim, S.D.K. Min, Thin Solid Films 279 (1996) 1–3.
[40] I. Barin, Thermochemical Data of Pure Substances, 3rd ed., VCH, Weinheim, Basel, 1995.